Thermohaline circulation in marginal seas

Michael A. Spall
Department of Physical Oceanography
Woods Hole Oceanographic Institution
Woods Hole, MA 02543

submitted to JMR: August 14, 2002

mspall@whoi.edu

Abstract.

The thermohaline circulation in an idealized marginal sea is studied using both numerical and analytical models. The circulation is forced by repeating an annual cycle of cooling in the interior of the marginal sea for 2 months and turning off the surface forcing for 10 months. The marginal sea is connected to an open ocean through a narrow strait, thus providing a means to equilibrate the cooling within the marginal sea by exchange with the open ocean. The resulting upper ocean circulation consists of a warm boundary current that flows into the marginal sea through the strait that is gradually eroded as it circulates cyclonically around the marginal sea. The deep circulation is in the opposite sense. The interior of the marginal sea is relatively cold and has a closed cyclonic circulation. The mean downwelling is concentrated within a narrow boundary layer that, for a Laplacian diffusion parameterization of subgridscale mixing of density and momentum, has a width of $L_d\sigma^{1/2}$ and an along-boundary decay scale of $L_d\sigma^{3/2}E^{-1}$, where L_d is the internal deformation radius, σ is the horizontal Prandtl number, and E is a horizontal Ekman number. The net downwelling outside of this boundary layer is very small at all times. The heat balance near the boundary is between vertical advection and horizontal diffusion at scales smaller than the mesoscale. In the interior, cooling by surface forcing and vertical convection is balanced by horizontal eddy fluxes. For some configurations, these eddy fluxes are characterized by very low frequency oscillations (periods of 1-10 years) in the gyre-scale circulation. One of the main results of this study is that the downwelling in the marginal sea is concentrated near the boundaries and depends on details of the mixing of momentum and density on scales smaller than the mesoscale. This suggests that, in addition to resolving the mesoscale eddy field, improved parameterizations of submesoscale mixing are needed to properly represent the circulation in marginal seas and the downwelling limb of the thermohaline circulation.

1 Introduction

Semi-enclosed marginal seas are often regions of a net buoyancy loss due to either atmospheric cooling or evaporation. Prominent examples include the Mediterranean Sea, the Red Sea, and the Adriatic Sea. For cases in which the marginal sea is connected to the open ocean by a single narrow and/or shallow strait, this net surface buoyancy flux is balanced by a lateral advection of buoyancy through the strait. Typically, relatively warm, fresh water is advected into the marginal sea through an upper ocean boundary current. These waters are made more dense within the marginal sea by air-sea exchange and return to the open ocean as a dense bottom current. The mass exchange between the basins is often quite small, while the net surface buoyancy flux in the marginal sea can be large. This results in temperature and salinity signatures of the product water masses that are quite distinct from the water properties of the open ocean. The spread of these waters away from the outflow can be clearly seen on property maps at depth in the open ocean.

The circulation that closes this inflow of light water and outflow of dense water within the marginal sea will be called the marginal sea thermohaline circulation. It is clear that the thermohaline circulation represents both a vertical buoyancy flux and a vertical mass (or volume) flux. As discussed by Spall and Pickart (2001), the vertical buoyancy flux and the vertical mass flux need not take place in the same location or be carried out by the same physical processes. There has been much recent interest in where and how the upwelling limb of the thermohaline circulation is closed, but relatively little attention has been paid to what controls the downwelling limb of the thermohaline circulation.

Buoyancy loss to the atmosphere can result in statically unstable density profiles and intense vertical mixing on very small scales (Killworth 1983, Marshall and Schott 1999). Laboratory and modeling studies have shown that such regions of buoyancy loss drive dense waters downward in narrow plumes of O(1 km) width, and lighter waters upward over larger scales between the plumes (Marshall and Schott 1999). This process results in a strong

vertical buoyancy flux with very little net vertical mass flux. If the depth to which vertical convection varies spatially, either due to variable buoyancy flux or spatially variable stratification in the ocean, geostrophic rim currents will develop over an inertial time scale. Sufficiently strong baroclinic shears in these rim currents can become baroclinically unstable and produces intense baroclinic eddies (Helfrich and Send 1988, Hermann and Owens 1993, Visbeck et al 1996). For cases of weak background flows, the lateral buoyancy flux carried by these eddies has been shown to play a crucial role in the buoyancy budget by offsetting the buoyancy flux with the atmosphere (Visbeck et al. 1996). However, each of these studies was relatively short in duration and considered only an effectively infinite domain and so could not close the buoyancy budget.

For semi-enclosed seas connected to the open ocean through a narrow strait, the net buoyancy loss in the marginal sea must ultimately be balanced by advection through the strait. The waters are carried to and from the strait within the marginal sea by boundary currents. This raises several questions. How is the lateral heat transport carried by eddies in the ocean interior communicated to the boundary currents? Where and by what means is the vertical mass flux achieved? How does this differ from the vertical heat flux?

This study attempts to provide insights into these questions in an idealized, but geophysically relevant, context. The approach makes use of both numerical and analytic models to describe the circulation and relate it to the basic parameters of the system. Buoyancy forcing is applied to a marginal sea, which is connected to an effectively infinite open ocean through a narrow strait. The open ocean provides a souce of light water with which to close the heat budget, and so allows for equilibrium solutions. The nature of the exchange between the marginal sea and the open ocean is not imposed, but instead emerges as part of the solution. The inclusion of lateral boundaries and the ability to resolve baroclinic instabilities and eddies are important aspects of the model formulation.

2 Thermohaline circulation in an idealized marginal sea

The thermohaline circulation in an idealized semi-enclosed marginal sea will be explored using the MIT primitive equation numerical model (Adcroft et al. 1997). The model solves the momentum and density equations using level (depth) coordinates in the vertical and a staggered C-grid in the horizontal. The model retains a free surface. A linear equation of state is used so that density is proportional to temperature as $\rho = \rho_0 - \alpha(T - T_b)$, where ρ_0 is a reference density for seawater, $T_b = 4$ is the initial temperature at the bottom, and the thermal expansion coefficient $\alpha = 2 \times 10^{-4}$ g cm^{-3}C^{-1}. The model is initialized at rest with a uniform stratification such that $T_0(z) = T_b + \partial T/\partial z(z_b - z)$, with the bottom depth $z_b = 1000$ m and vertical gradient $\partial T/\partial z = 1.875 \times 10^{-3}$ °C m^{-1}. The initial temperature at the surface is 5.875. The model is configured with uniform horizontal grid spacing of 5 km and 12 levels in the vertical with thickness 83 m. The Coriolis parameter is 10^{-4} s^{-1} and constant, so that the internal deformation radius based on this open ocean stratification is approximately 10 km. All calculations presented here have a flat bottom.

The model domain consists of a circular basin 500 km in diameter connected to an "open ocean" through a channel 100 km wide. The temperature in the open ocean region is restored towards the initial uniform stratification $T_0(z)$ with a time scale of 20 days. In this way, the properties of the water flowing into the marginal sea are fixed, independent of what processes take place in the marginal sea. The model is forced by cooling over a region 200 km in diameter in the center of the marginal sea. A cooling of 400 W m^{-2} is applied for two months and then turned off for 10 months. This annual cycle is repeated for a period of 10 years.

Subgridscale processes are parameterized using Laplacian viscosity and diffusion in both the horizontal and vertical directions. The vertical diffusion coefficient is 10^{-5} m^2 s^{-1}, while the vertical viscosity coefficient is 2×10^{-4} m^2 s^{-1}. Lateral boundary conditions are no-slip

and there is no heat flux through the solid boundaries. The horizontal mixing parameterization emerges as an important factor in the marginal sea circulation. It is emphasized here that the numerical model resolves the internal deformation radius and mesoscale eddies. The horizontal mixing parameterizes mixing processes on scales smaller than the mesoscale. While horizontal Laplacian operators are no doubt an oversimplification of the real mixing processes, little is known about how waters mix at such scales near lateral boundaries. This approach at least allows some analytic progress and it highlights the importance of these poorly understood processes for the large-scale thermohaline circulation.

This configuration and forcing are not intended to represent a realistic seasonal cycle or mean circulation in the marginal sea. They are designed to help understand how heat loss and isolated deep convection in the interior of the marginal sea interact with a lateral boundary and the open ocean. This configuration can be viewed as the simplest extension of the isolated deep convection calculations of Visbeck et al. (1996), Madec et al. (1991), Herman and Owens (1993), and others, in which the heat budget can be closed through a non-local source of warm water.

The basin-averaged temperature in the marginal sea as a function of time is shown in Fig. 1. There is a net annual mean heat loss in the marginal sea during the first approximately 5 years of integration, afterwhich the annual trend in the basin-averaged temperature is very small. The heat loss at the surface in the marginal sea is balanced by lateral advection from the open ocean through the strait. Most of the analyis in this paper are carried out over the final three years of integration, when the long-term trend in basin-averaged temperature is small.

The mean sea surface temperature over the final three years of integration is shown in Fig. 2. The interior of the marginal sea is approximately 0.75° C cooler than the open ocean. The warm water from the open ocean flows into the basin along the right-hand side of the marginal sea in a boundary current approximately 50 km wide. This temperature

signal is eroded as it penetrates into the marginal sea so that the temperature along the boundary is nearly constant around the left-hand side of the basin. There are also some closed temperature contours in the interior of the basin indicative of a weak doming of the isopycnals there.

The basic vertical stratification in the marginal sea is indicated by the zonal section through the mid-latitude of the marginal sea shown in Fig. 3a. The isopycnals are steeply sloped within 50 km of the boundaries. There is a region approximately 100 km wide, between a radius 100 km and 200 km, in which the isotherms are nearly flat. The isotherms are weakly domed within the cooling region in the interior. The stratification is strongest near the surface and near the boundaries and weaker at depth and in the interior.

The meridional velocity (Fig. 3b) shows baroclinic boundary currents in geostrophic balance with the sloping isopycnals near the boundaries. The circulation in the upper ocean is cyclonic and the circulation in the deep ocean is anticyclonic, as expected from angular momentum considerations (Whitehead et al. 1998). There is also a weak, nearly barotropic southward flow through the interior of the basin flanked by barotropic northward flows on either side.

The mean potential vorticity $q = (f_0+\zeta)\partial\rho/\partial z$, where $\zeta = \partial v/\partial x - \partial u/\partial y$ is the relative vorticity, along this section is shown in Fig. 3c. The deep potential vorticity is very small as a result of deep convection when buoyancy-forcing is active. Although deep convection occurs only where cooling is applied, the broad signal of low potential vorticity at depth indicates that this convectively generated water mass spreads towards the boundaries. The potential vorticity near the surface is much larger, and is a maximum in an annulus between radii 100 km and 200 km. The potential vorticity in the mean is dominated by the vertical stratification, contributions from relative vorticity are neglegible. The potential vorticity in the open ocean is 1.7 and uniform throughout the water column. The deep potential vorticity

is lower than the open ocean value while the upper ocean and near boundary regions are higher than found in the open ocean.

The source of this high stratification is indicated by a synoptic view of the temperature and potential vorticity at 41.7 m just after cooling has ceased in winter (Figs. 4, 5). Deep convection occurs each winter within the cooling region, resulting in weakly stratified, dense water near the surface. The dense upper ocean waters spread outwards from the cooling region in the form of mesoscale eddies, consistent with the studies of Madec et al (1991), Helfrich and Send (1988), Hermann and Owens (1993), Visbeck et al. (1996), Marshall and Schott (1999). There is strong variability all along the perimeter of the dense water, with very strong density gradients in the region where the warm water flows into the basin.

The potential vorticity (Fig. 5) has low values in the basin interior, where cooling has driven deep convection, and within many of the eddies. However, along the perimeter of the eddies and fronts the potential vorticity is much larger than in the surrounding waters. This high potential vorticity results from increased stratification, not from relative vorticity. The meandering front between the dense water in the interior and the warm water entering from the open ocean contains a nearly continuous band of high stratification. This did not originate in the restoring region of the open ocean, but was instead generated within the marginal sea as part of the restratification process. This is also evident from the regions of high potential vorticity around the eddies in the northern part of the marginal sea, well away from the open ocean. The annulus of high potential vorticity found in the marginal sea after restratification is also found if there is no open ocean, confirming that the basic process is inherent to the restratification by baroclinic instability. This may be thought of as a manifestation of having a variable temperature along the surface, as discussed by Pedlosky (1963), Bretherton (1966) and Legg and Marshall (1993).

The downwelling limb of the thermohaline circulation is revealed by the mean vertical velocity integrated in the azimuthal direction as a function of radius and depth in Fig. 6. The

vertical velocity is a weak function of distance along the marginal sea boundary, as discussed further below, but integrating reduces the grid-scale spatial variability of the vertical motions in the interior regions where overturning is active and clearly demonstrates the dominant pattern of vertical velocity. The large-scale mean vertical motions are everywhere downward and concentrated within approximately 20 km of the perimeter of the marginal sea. The downwelling is also a maximum near the mid-depth of the basin and decreases towards zero at the surface and bottom. The downwelling in the interior, within the cooling region, is neglegible.

The vertical transport as a function of time is shown in Fig. 7 for the innermost 100 km (where the cooling is active) and for the outer 150 km. It takes approximately 5 years for the magnitude of the downwelling within the marginal sea to reach a quasi-steady state. This is consistent with the spin-up time for the basin-averaged temperature in Fig. 1. The mean downwelling transport between years 7 and 10 is 0.49 Sv, with over 95% taking place within 25 km of the marginal sea boundary. The downwelling in the interior is quite small at all times of the year.

There is a clear seasonal signal, with maximum downwelling occuring 30-60 days after cooling has ceased. This is approximately the time it takes for eddies formed in the interior to reach the boundaries. As discussed further in Section 3, it is the interaction of the eddies with the boundaries that drives the vertical motion. The magnitude of the downwelling decreases slowly for the remainder of the year, but is always negative. The seasonal cycle is approximately 40% of the mean downwelling rate. The spreading of the dense waters by mesoscale eddies and their evential dissipation introduces a slow time scale to the thermohaline circulation such that the net downwelling in the basin varies much more slowly than its production in winter.

This finding differs from the traditional view that the downwelling limb of the thermohaline circulation takes place in the interior regions of deep convection (e.g. Schmitz and

McCartney 1993). There is strong vertical mixing and vertical heat flux in the region of cooling, but the vertical mass flux, when integrated over scales larger than a single plume, is small. This is consistent with the high resolution nonhydrostatic modeling study of Send and Marshall (1995). However, it is found here that the downwelling in the interior remains small not only during the initial active phase of deep convection, but also throughout repeated cycles of deep convection and restratification due to baroclinic eddies.

The process of baroclinic instability during restratification converts potential energy into kinetic energy, thereby allowing dense water to sink and light water to rise. However, the constraints imposed by geostrophy do not allow the isopycnals of the spreading dense water in the interior to become horizontal – the thermal wind relation requires that the kinetic energy of the eddies be balanced by sloping isopycnals (see, for example, McWilliams 1988). The amount of the original dense water column that sinks depends on the size of the eddies relative to the internal deformation radius; larger eddies result in less slumping and more of the dense water trapped in cyclonic domes. The finding here is that most of the restratification process takes place by a predominantly horizontal exchange between the stratified region near the boundaries and the interior deep convection sites. This is evident by the cold water seen near the surface outside of the cooling region in Fig. 4. The cold water in these eddies ultimately downwells, and its potential energy is dissipated, when it interacts with the boundaries. The dynamics and thermodynamics that control this downwelling and eddy decay will be investigated further in the remainder of the paper.

3 A simple model of the near-boundary thermohaline circulation

The downwelling component of the thermohaline circulation in the numerical model is concentrated near the horizontal boundaries. In this section, a simple analytic model is developed to aid in understanding how this downwelling (amplitude and spatial scales) depends

on the basic parameters of the system. For simplicity, the fluid is represented by two isopycnal layers of density ρ_1 and ρ_2. The linear vorticity equation with lateral viscosity may be written for each of the moving layers.

$$(-1)^n \frac{f_0 w}{h_n} = -A_h \nabla^2 \zeta_n, \tag{1}$$

where f_0 is the Coriolis parameter, assumed here to be constant, A_h is the lateral viscosity coefficient, $\zeta_n = \partial v_n/\partial x - \partial u_n/\partial y$ is the relative vorticity of layer n, v_n, u_n are the meridional and zonal velocities. The vertical velocity w is defined at the layer interface. The sum of the layer thicknesses $h_1 + h_2 = 2H$, where $2H$ is the bottom depth, taken here to be constant. For simplicity, it is assumed that the layer thicknesses in the open ocean are each equal to H. This boundary condition is imposed in the analytic model by setting the layer thicknesses $h_n = H$ on the boundary at the inflow to the marginal sea ($x = y = 0$). For a flat bottom, and in the absence of wind-forcing or a bottom Ekman layer, the vertical velocity at the surface and bottom are zero. Cartesian coordinates are used with x perpendicular to the boundary, $x < 0$ extending into the ocean interior, and y parallel to the boundary.

The model is forced by restoring the upper layer thickness h_1 towards a specified thickness $\mathcal{H}$ with time scale τ. This is intended to represent the advection of cold water of upper layer thickness $\mathcal{H}$, formed in the interior during deep convection, towards the boundaries by mesoscale eddies. For an upper layer thickness $h_1 > \mathcal{H}$, this causes the upper layer to become thinner and the lower layer to become thicker. Because the lower layer is of higher density, this represents cooling and a downward mass flux. This mass exchange may be expressed in terms of the cross-isopycnal velocity w^* at the layer interface as

$$w^* = \frac{\mathcal{H} - h_1}{\tau} = \frac{-P}{\tau g'}, \tag{2}$$

where P is a perturbation pressure in the upper ocean relative to the deep ocean and g' is the reduced gravity between the upper layer and the lower layer.

It is assumed that the meridional velocity is in geostrophic balance so that $v_1 - v_2 = P_x/f_0$. Anticipating an eastern boundary current structure, it is further assumed that $v_x \gg u_y$. If the layer 2 vorticity equation is subtracted from the layer 1 vorticity equation, a single equation for the perturbation pressure P may be written as

$$P_{xxxx} + \frac{2f_0^2}{g'H\tau A_h}P = 0. \tag{3}$$

The vertical stretching term has been linearized with respect to the layer thickness, so that H is used in place of h_n. It has also been assumed that the cross isopycnal velocity w^* is the same as the vertical velocity w. These assumptions are valid as long as the perturbation of the layer interface due to the geostrophic flow is small compared to the basic stratification. This condition is well met near the boundaries, as shown in Fig. 3.

It is useful to nondimensionalize the equation with the following scaling:

$$P \propto V f_0 L_d \qquad\qquad x, y \propto L_d = (g'H)^{1/2}/f_0, \tag{4}$$

where V is a characteristic velocity scale and L_d is the internal deformation radius. The nondimensional vorticity equation is now written as

$$P_{xxxx} + (L_d/\delta)^2 P = 0, \tag{5}$$

where $\delta = (A_h\tau)^{1/2}$. The width of the boundary layer depends on the time constant τ. The value and parameter dependence of τ depends on the processes that control the mixing of density at sub-mesoscale scales. The derivation will be carried out keeping τ as a general

free parameter. A specific form of density mixing will be specified after the analytic solution is complete.

It is assumed that the solution can be separated into an exponential in the offshore direction x and an undetermined function of the alongshore direction y.

$$P(x, y) = F(y)e^{ikx} \tag{6}$$

Substitution of (6) into (5) results in an equation for the complex roots k:

$$k^4 + (L_d/\delta)^2 = 0. \tag{7}$$

There are two roots of (7) that remain bounded for $x < 0$.

$$k_{1,2} = \sqrt{2}/2(L_d/\delta)^{1/2}(\pm 1 - i) \tag{8}$$

The dimensional boundary layer width is thus proportional to $(L_d\delta)^{1/2}$. The pressure may be written as the sum of two boundary layers, each with unknown meridional dependence, as

$$P(x, y) = F(y)e^{ik_1 x} + G(y)e^{ik_2 x}. \tag{9}$$

The relationship between $F(y)$ and $G(y)$ is required by the no-slip boundary condition to be

$$G(y) = -k_1/k_2 F(y). \tag{10}$$

A non-dimensional equation for the variation in pressure along the boundary, where $u = 0$, may be derived by subtracting the layer 2 meridional momentum equation from the layer 1 meridional momentum equation,

$$P_y = EP_{xxx}, \tag{11}$$

where $E = A_h/f_0 L_d^2$ is a horizontal Ekman number. Substitution of (9) and (10) into (11) results in an equation for $F(y)$.

$$F_y - iEk_1k_2(k_1 + k_2)F = 0 \tag{12}$$

The solution for F is simply

$$F = e^{-\sqrt{2}(L_d/\delta)^{1.5}Ey}P_0 \tag{13}$$

where the amplitude has been set to P_0 at $y = 0$.

The full solution for the perturbation pressure is now written as

$$P = \frac{k_2}{k_2 - k_1}e^{-\sqrt{2}(L_d/\delta)^{1.5}Ey}\Big(e^{ik_1x} - \frac{k_1}{k_2}e^{ik_2x}\Big)P_0 \tag{14}$$

The perturbation pressure P determines the baroclinic shear between layers 1 and 2. For this simple application with a flat bottom and no stress at the surface or bottom, the depth averaged flow vanishes, so that the flow is purely baroclinic and $v_1 = -v_2$, $u_1 = -u_2$.

The time scale τ depends on how temperature (or pressure) anomalies are eroded near the boundaries. If the temperature equation is forced directly by heat exchange with the atmosphere near the boundaries, then this time scale would depend on how strongly the atmosphere cools (or heats) the ocean. For the present case, there is no direct forcing from the atmosphere near the boundaries. Although this is imposed here by restricting the heat

flux to the interior of the marginal sea, this may also be the case at mid-depths if the near boundary region is strongly stratified by boundary currents. In this case, thermal anomalies will be eroded by small-scale diffusion processes. The dynamics that control such mixing processes are not well understood, but for simplicity it is assumed here that temperature anomalies are eroded by a horizontal Laplacian diffusion. Note again that this diffusion is assumed to be taking place on scales smaller than the mesoscale. In this case, the time scale over which the temperature anomalies are eroded is

$$\tau = \frac{\delta^2}{A_T} = \frac{L_d^2 A_h}{A_T^2}, \tag{15}$$

where A_T is the Laplacian diffusion coefficient.

The dimensional boundary layer width is then

$$\delta = L_d \sigma^{1/2}, \tag{16}$$

where $\sigma = A_h/A_T$ is the Prandl number. This boundary layer width is the same as was derived by Barcilon and Pedlosky (1967) using continuously stratified momentum and density equations. Whitehead and Pedlosky (2000) found evidence for such boundary layers and their impact on the basin-scale circulation in a series of laboratory experiments in which the basin was heated from the side. It is worth noting that Barcilon and Pedlosky (1967) and Whitehead and Pedlosky (2000) used a different parameterization for the vertical velocity, which resulted in a second order partial differential equation for pressure, yet find the same boundary layer width, suggesting that the basic result is not overly sensitive to the specific form of (2). Those studies were for axially symmetric basins, so that there was no variation in the pressure along the boundary. For a marginal sea connected to an open ocean, the pressure does vary along the boundary within the marginal sea. The dimensional e-folding scale along the boundary over which the pressure signal decays is, from (13),

$$\gamma = \frac{L_d \sigma^{1.5}}{\sqrt{2}E} = \frac{\delta}{\sqrt{2}E_T}, \tag{17}$$

where $E_T = A_T/f_0 L_d^2$ is a thermal Ekman number.

An example of the pressure, or thickness of the upper layer, is shown in Fig. 8 for $P_0 = 1$, $\sigma = 1$ and $E = 0.00125$. There is a narrow boundary current of width $O(L_d)$ flowing towards the north. The pressure contours intersect the eastern boundary, with the meridional gradient along the boundary decreasing with distance northward. The e-folding distance for the pressure signal to be eroded along the boundary is $\gamma = 565 L_d$. Because the flow parallel to the boundary is in geostrophic balance, the intersection of pressure contours with the side boundary implies that there is downwelling within the boundary current. The strength of the downwelling is proportional to the pressure anomaly; it is concentrated within δ of the side wall and decays along the boundary with scale γ.

The total amount of downwelling within a marginal sea can be calculated as a function of the perimeter of the marginal sea L_y/L_d and the nondimensional along-boundary decay scale $\sigma^{1.5}E^{-1}$, as shown in Fig. 9. The pressure anomaly at the inflow to the basin P_0 is set to 1 and it is assumed that the width of the basin is large compared to the boundary layer width δ. The dependence of the total downwelling rate on these parameters falls into two regimes. For small basins in which $L_y/L_d < \sigma^{1.5}E^{-1}$, the downwelling increases linearly with basin perimeter and is independent of the along-boundary decay scale. In this limit, the downwelling is uniform along the boundary and the total overturning is controlled by the boundary layer width δ and the length of the basin perimeter. For large basins, such that $L_y/L_d > \sigma^{1.5}E^{-1}$, the downwelling is independent of the basin size and depends only on the along boundary decay scale. This is because all of the water flowing into the basin downwells before the boundary current has flowed all the way around the marginal sea. If the decay scale is large, then more water downwells near the boundary.

4 Parameter sensitivities

The two characteristic length scales derived from the analytic model represent the boundary layer width and the along-boundary decay scale. A series of calculations have been carried out with the MIT primitive equation model in which the Coriolis parameter, lateral viscosity, lateral diffusivity, stratification, and meridional variation in the Coriolis parameter have been varied. These runs are summarized in Table 1. Unless stated otherwise, all other parameters are as in the standard run from Section 2 (run# 1). The boundary layer width was diagnosed by first calculating the azimuthally integrated vertical velocity, as in Fig. 6. The boundary layer width was defined as the distance from the boundary at which the downwelling was reduced to 10% of its maximum value. The width of the boundary layer in the model is compared to the theoretical estimate of $L_d\sigma^{1/2}$ in Fig. 10a. There is in general close agreement between the model and theory. The model boundary layer width is consistently wider than the theory by a factor of approximately 2, as expected from Fig. 8.

This close comparison indicates that the basic balance represented in the analytic model is active in the full primitive equation model. This is verified by the heat budget analysis in the following section. The downwelling is concentrated near the boundary because that is the only place where both the vertical advection of temperature can be balanced by a lateral diffusion of temperature *and* the vorticity generated by this vortex stretching can be balanced by a lateral vorticity flux into the boundary. The presence of significant viscosity also causes the geostrophic balance in the along-boundary direction to break down, thus allowing for significant vertical motions. The width of the downwelling region increases with increasing A_h because vorticity is dissipated more effectively. The width decreases with increasing A_T because the vertical velocity (and vortex stretching) increases as the lateral diffusion of temperature increases. All of the vertical motion is concentrated near the horizontal boundaries because this is the only place where vorticity can be effectively dissipated. For this reason, other parameterizations of subgridscale mixing would also favor the deformation

radius and near boundary region for the downwelling limb of the thermohaline circulation. As discussed by Send and Marshall (1995) and Spall and Pickart (2001), even comparatively weak vertical motions in the interior would lead to very unrealistic horizontal recirculations as a consequence of vortex stretching.

The along-boundary decay scale found in the model is compared to that predicted by the theory in Fig. 10b. The decay scale in the model is defined as the along-boundary distance at which the temperature anomaly on the boundary at the inflow to the marginal sea is reduced by a factor of e^{-1}. This temperature anomaly is defined as the difference between the surface temperature on the boundary at the inflow to the marginal sea (which is nearly the same as the open ocean surface temperature) and the mean surface temperature just outside the boundary layer (at a distance of 2δ towards the interior). The decay scale varies by an order of magnitude, roughly between 100 km and 1000 km, and there is reasonably good agreement between the numerical model and the theory. This favorable comparison again supports the basic dynamics of the analytic model.

The comparison between the total downwelling amplitude in the numerical model and that predicted by the analytic solution is shown in Fig. 10c. The downwelling rate in the model varies between 0.25 Sv and 0.62 Sv, where 1 Sv = $10^6 \mathrm{m}^3\ \mathrm{s}^{-1}$. The analytic model produces similar downwelling rates, although it underpredicts the downwelling at the lower values. The downwelling within the marginal sea decreases with increasing Coriolis parameter and with decreasing depth. It is less sensitive to variations in the diffusion and viscosity coefficients, although the width and along-boundary decay scale clearly do depend on these parameters.

Examples of the surface temperature in two extreme cases are shown in Figs. 11 and 12. The along-boundary decay scale for the case with horizontal viscosity increased to 150 $\mathrm{m}^2\ \mathrm{s}^{-1}$ (Fig. 11) is 1100 km, about twice the 631 km for the standard case shown in Fig. 2. The warm boundary current extends much farther into the marginal sea than for the previous

case. The level 1 temperature for the calculation with an increase in the horizontal diffusion to 150 m^2 s^{-1} is shown in Fig. 12. For this case, the theoretical estimate of the decay scale is only 125 km. The temperature signal from the open ocean is eroded very quickly upon entering the marginal sea. The remainder of the boundary in the marginal sea is much colder and of nearly uniform temperature. These results demonstrate that the structure of the boundary current system and the thermohaline circulation itself are very sensitive to the diffusive processes that happen on scales smaller than the mesoscale. Very different results are found when the Laplacian viscosity or diffusion are varied by only a factor of 3. These calculations are not intended to be realistic represention of marginal sea thermohaline circulations, but rather to emphasize the importance of mixing processes near the boundaries at scales less than the deformation radius for the basin-scale thermohaline circulation.

The analytic model can also be used to estimate the total downwelling within the marginal sea. The downwelling is calculated from (2) and the analytic solution for the pressure (14). The inflow pressure anomaly is calculated from temperature as $P_0 = g'\delta T(\partial T/\partial z)^{-1}$, where $\delta T = T_0 - T_i$ is the difference between the surface temperature on the boundary at the inflow to the marginal sea and the temperature at the surface 2δ towards the interior. The reduced gravity $g' = 0.5\Delta T\alpha g/\rho_0$, where $\Delta T = T_0 = T_b$ is the change in temperature from the surface to the bottom of the open ocean. The analytic boundary layer solution is integrated along a boundary of length $2\pi R_0$, where $R_0 = 250$ km is the radius of the marginal sea.

5 Heat balances

The balance of terms in the heat equation are useful to ellucidate the different dynamical regimes within the marginal sea. The temperature equation solved by the MIT primitive equation model is written as

$$\frac{\partial T}{\partial t} = -\nabla \cdot (\vec{\mathbf{v}} T) - \frac{\partial (wT)}{\partial z} + A_T \nabla^2 T + K_T \frac{\partial^2 T}{\partial z^2}, \tag{18}$$

where $\vec{\mathbf{v}} = u\vec{\mathbf{i}} + v\vec{\mathbf{j}}$ is the horizontal velocity vector. The advection terms (first and second on the right hand side of (18)) are further decomposed into mean and eddy components:

$$\nabla \cdot (\vec{\mathbf{v}} T) + \frac{\partial (wT)}{\partial z} = \nabla \cdot (\overline{\vec{\mathbf{v}}' T'}) + \frac{\partial (\overline{w' T'})}{\partial z} + \nabla \cdot (\overline{\vec{\mathbf{v}}}\ \overline{T}) + \frac{\partial (\overline{w}\ \overline{T})}{\partial z}, \tag{19}$$

where the overline denotes a time average and primes are deviations from the time mean.

The heat balance at 208 m depth is shown in Fig. 13 for the years 7-10 of the central calculation. The balances may be broken down into several distinct regimes. Near the boundary the primary balance is between horizontal diffusion and advection, where the advection in this case is dominated by vertical advection. This is the same balance as was assumed in the derivation of the analytic model in Section 2. Just to the right of the inflow to the marginal sea the eddy fluxes are cooling near the boundary and heating towards the interior. This is the signature of baroclinic instability of the inflowing boundary current, as suggested by the meandering in Fig. 4.

The balance in the interior, within the cooling region, is between both mean and eddy advection and vertical diffusion. The vertical diffusion is a result of the buoyancy forcing at the surface. The vertical mixing due to convective instability is parameterized in this calculation by increasing the vertical diffusion coefficient to 1000 $\mathrm{m}^2\ \mathrm{s}^{-1}$ when $\partial \rho / \partial z > 0$. The active role of the mean advection is different from what has been found for the previously cited calculations in which cooling is applied over a circular region for a relatively short time.

In the interior, it is the horizontal component of the advection that is warming the cooling region and cooling the basin to the south of the cooling region. This is demonstrated by a plot of the mean horizontal velocity and temperature at this depth in Fig. 14. There is a large-scale cyclonic circulation in the southeast region of the marginal sea that is advecting

warm water from the near boundary region into the interior and through the cooling region. The coldest water is found near the southern rim of the cooling disk, just where the contribution due to mean advection changes sign from heating to cooling. The flow in the interior is nearly barotropic, as indicated in the zonal section shown in Fig. 3. The influence of this southward mean flow is evident in the snapshot of temperature and potential vorticity just after the cooling has ceased in Figs. 4 and 5 by the elongated southward extension of the cold, low potential vorticity water.

The net influences of vertical diffusion, mean advection, and eddy advection within the cooling region are shown in Fig. 15a as a function of depth. Mean advection is larger than the eddy fluxes at all depths, and dominates the eddy contribution at mid-depths. Because the cyclonic circulation shown in Fig. 14 is largely barotropic, it plays an important role in the heat budget throughout the water column. The cooling by advection of this cold patch towards the southern boundary of the marginal sea is offset by an eddy flux of warm water towards the interior – the baroclinic instability of the inflowing marginal sea water. However, this mean flow is in reality an aliasing of a very low frequency oscillation of the barotropic circulation in the interior of the basin. This is demonstrated by the balance of terms within the cooling region calculated for the period between year 10 and year 30, based on a restart of the central calculation at year 10. The contribution of the mean advection in this case is quite small over the whole water column (Fig. 15b). Calculations for short periods (1 to 3 years) during this time period give results similar to that found for years 7-10, so the difference is not due to the choice of a different time period but rather due to the longer averaging period. The eddy flux is composed of both high frequency mesoscale eddies generated during the restratification process and very low frequency (1-10 year) oscillations in the barotropic flow in the basin interior. A similar role for low frequency oscillations is found for a calculation with cooling uniform in time at 1/6 the strength applied here.

The existence of these low frequency oscillations is strongly dependent on the model configuration and parameters. They are greatly reduced if the flow is made more symmetric

around the perimeter of the marginal sea. This can be accomplished by closing the strait, in which case there is perfect symmetry (although equilibrium solutions are no longer possible), or by increasing the viscosity, as in Fig. 11. In either case the contribution from mean advection in the interior is neglegible over a 1-3 year averaging period. The low frequency oscillations are also eliminated when the Coriolis parameter varies with latitude as $f = f_0 + \beta y$, where $\beta = 2 \times 10^{-11}$ m^{-1} s^{-1}. This indicates that the oscillations are at larger scales than $(V/\beta)^{1/2}$, the scale at which wave dynamics dominate over advective dynamics (Rhines 1975). For a mean flow of $V = 0.02$ m s^{-1} and $\beta = 2 \times 10^{-11}$ m^{-1} s^{-1}, this transition occurs at approximately 30 km. Large-scale, weak features subject to only weak forcing can not persist for long periods on a beta-plane. This suggests their role in the real ocean may be limited to very small scales or high latitude regions, where β is small.

6 Summary and Conclusions

The thermohaline circulation in an idealized marginal sea has been studied using both numerical and analytical models. An important aspect of the model configuration is that the marginal sea is connected to an open ocean through a narrow strait, so that the net heat loss in the marginal sea can be balanced by advection through the strait and the equilibrium circulation can be explored. The dense water formed in the interior is communicated to the boundary region by mesoscale eddies and, in some cases, low frequency oscillations of the basin-scale interior circulation. The circulation in the interior is weakly cyclonic, while near the boundary there is a cyclonic boundary current in the upper ocean and an anticyclonic boundary current in the deep ocean.

A dominant characteristic of the circulation is that essentially all of the downwelling is concentrated within a narrow boundary current that circulates cyclonically around the marginal sea. The downwelling in the interior of the marginal sea, where the buoyancy forcing is located, is nearly zero at all times of the year. A simple analytic model is used to

describe the dynamics of this downwelling region. For a Laplacian parameterization of subgridscale mixing of momentum and density, its width scales as $L_d\sigma^{1/2}$ and its along-boundary decay scale is $L_d\sigma^{3/2}E^{-1}$, where L_d is the internal deformation radius, σ is the horizontal Prandtl number, and E is a horizontal Ekman number. The important result here is not in the detailed prediction of these scales, which are dependent on the subgridscale parameterizations, but rather that the characteristics of the marginal sea thermohaline circulation and basin-scale density distribution depend on how mixing of density and momentum take place on scales less than the mesoscale and near lateral boundaries. It is expected that, even for other forms of subgridscale mixing, the downwelling limb of the thermohaline circulation will remain concentrated near the boundaries in narrow boundary currents of $O(L_d)$ width.

This study must be viewed as an initial attempt to understand what controls the downwelling limb of the thermohaline circulation in an ocean that permits mesoscale eddies. Perhaps the most unrealistic aspects of the model configuration are the lack of a topographic slope near the boundaries and the parameterization of submesoscale mixing using a Laplacian operator. Preliminary numerical calculations with a sloping bottom suggest that many aspects of the solution are similar to those reported here, namely that the downwelling remains concentrated near the (now sloping) boundaries in narrow regions of $O(L_d)$ width, but a detailed understanding of these results requires further study. It is hoped that the sensitivity of the basin-scale thermohaline circulation to small scale mixing processes will provide a motivation for improving our understanding of how water masses mix near lateral boundaries on spatial scales of $O(1$ km$)$.

Acknowledgments

This work was supported by the Office of Naval Research under Grant N00014-01-1-0165. This is Woods Hole Oceanographic Institution contribution number 10808.

References

Adcroft, A., C. Hill, and J. Marshall, 1997. Representation of topography by shaved cells in a height coordinate ocean model. Mon. Wea. Rev., *125,* 2293-2315.

Barcilon, V. and J. Pedlosky, 1967. A unified linear theory of homogeneous and stratified rotating fluids. J. Fluid Mech., *29,* 609-621.

Bretherton, F. P., 1966. Critical layer instability in baroclinic flows. Quart. J. R. Meteorol. Soc., *92,* 325-334.

Helfrich, K. and U. Send, 1988. Finite-amplitude evolution of two-layer geostrophic vortices. J. Fluid Mech., *197,* 331-348.

Hermann, A. J., and W. B. Owens, 1993. Energetics of gravitational adjustment for mesoscale chimneys. J. Phys. Oceanogr., *23,* 346-371.

Killworth, P. D., 1983. Deep convection in the world ocean. Rev. Geophysics, *21,* 1-26.

Legg, S. and J. Marshall, 1993. A heton model of the spreading phase of open-ocean deep convection. J. Phys. Oceanogr., *23,* 1040-1056.

McWilliams, J. C., 1988. Vortex generation through balanced adjustment. J. Phys. Oceanogr., *18,* 1178-1192.

Madec, G., M. Chartier, P. Delecluse, and M. Crepon, 1991. A three-dimensional numerical study of deep-water formation in the northwestern Mediterranean Sea. J. Phys. Oceanogr., *21,* 1349-1371.

Marshall, J. and F. Schott, 1999. Open-ocean convection: observations, theory, and models. Rev. Geophysics, *37,* 1-64.

Pedlosky, J., 1963. The stability of currents in the atmosphere and the ocean. Doctoral Thesis, Massachusetts Institute of Technology, 149 pp.

Rhines, P. B., 1975. Waves and turbulence on a beta-plane. J. Fluid Mech., *69,* 417-443.

Schmitz, W. J., and M. S. McCartney, 1993. On the North Atlantic circulation. Rev. Geophys., *31,* 29-49.

Send, U., and J. C. Marshall, 1995. Integral effects of deep convection. J. Phys. Oceanogr., *25,* 855-872.

Spall, M. A., and R. S. Pickart, 2001. Where does dense water sink? A subpolar gyre example. J. Phys. Oceanogr., *31,* 810-826.

Visbeck, M., J. Marshall, H. Jones, 1996. Dynamics of isolated convective regions in the ocean. J. Phys. Oceanogr., *26,* 1721-1734.

Whitehead, J. A., and J. Pedlosky, 2000. Circulation and boundary layers in differentially heated rotating stratified fluid. Dyn. Atmos. Oceans, *31,* 1-21.

Whitehead, J. A., G. K. Korotaev, S. N. Bulgakov, 1998. Convective circulation in mesoscale abyssal basins. Geophys. Astrophys. Fluid Dyn., *89,* 169-203.

RUN	f_0	A_h	A_T	Δ T	depth	β	downwelling	symbol	
1	1 e-4	50	50	1.875	1000	0	0.49	circle	
2	.5e-4	50	50	1.875	1000	0	0.55	asterisk	
3	2 e-4	50	50	1.875	1000	0	0.37	asterisk	
4	1 e-4	150	50	1.875	1000	0	0.49	square	
5	1 e-4	250	50	1.875	1000	0	0.51	square	
6	1 e-4	50	150	1.875	1000	0	0.49	triangle	
7	1 e-4	50	250	1.875	1000	0	0.62	triangle	
8	1 e-4	50	50	0.975	1000	0	0.66	plus	
9	1 e-4	50	50	1.875	500	0	0.31	diamond	
10	1 e-4	50	50	1.875	2000	0	0.54	diamond	
11	1 e-4	50	50	1.875	1000	2.e-11	0.45	cross	

Table 1: Model run parameters, total downwelling rate (Sv, 1Sv $=^1 0^6$ m^3 s^{-1}), and symbols used in Fig 10.

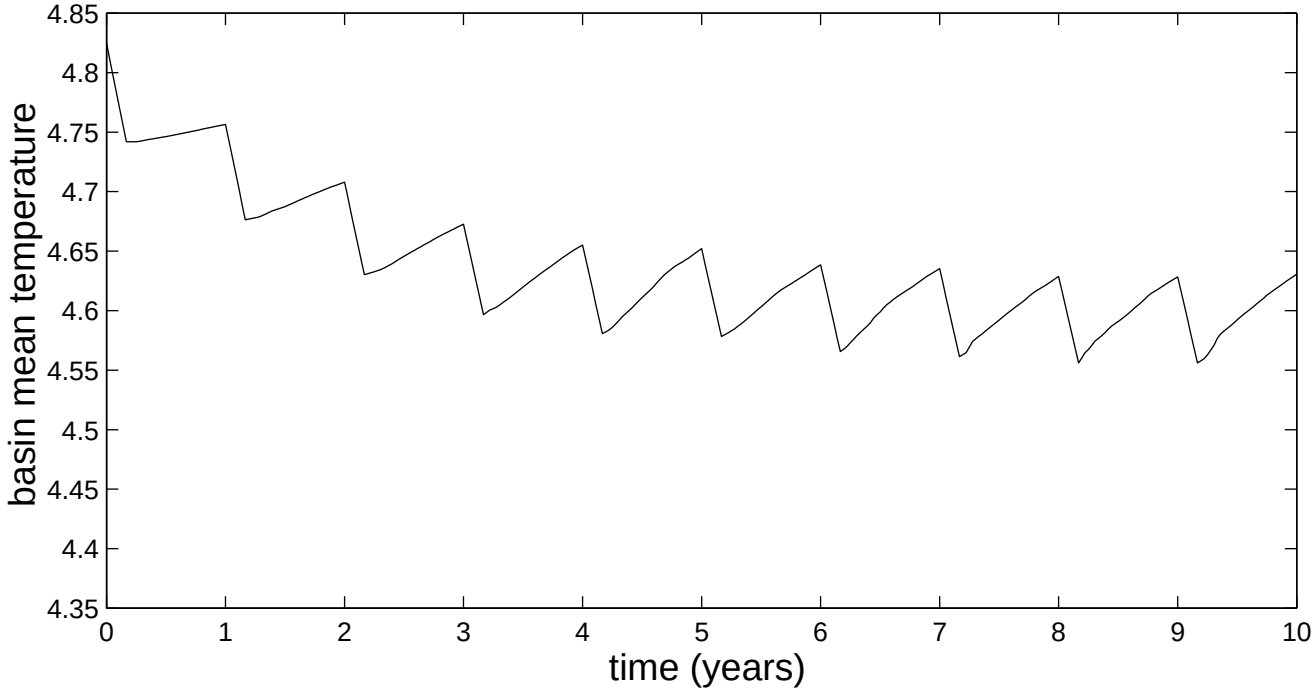

Figure 1: Basin-averaged temperature (° C) within the marginal sea as a function of time.

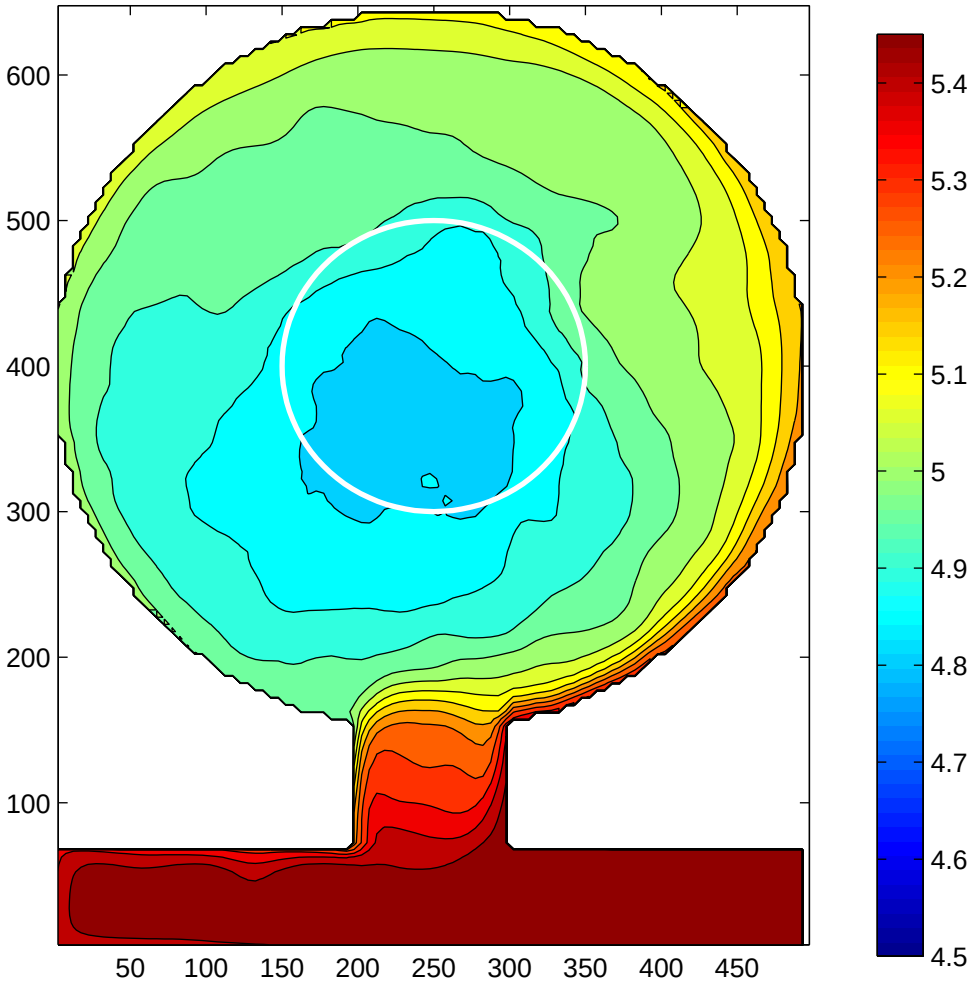

Figure 2: Mean temperature (° C) at 41.7m (model level 1) averaged over the final 3 years of integration. The region of cooling is indicated by the white line.

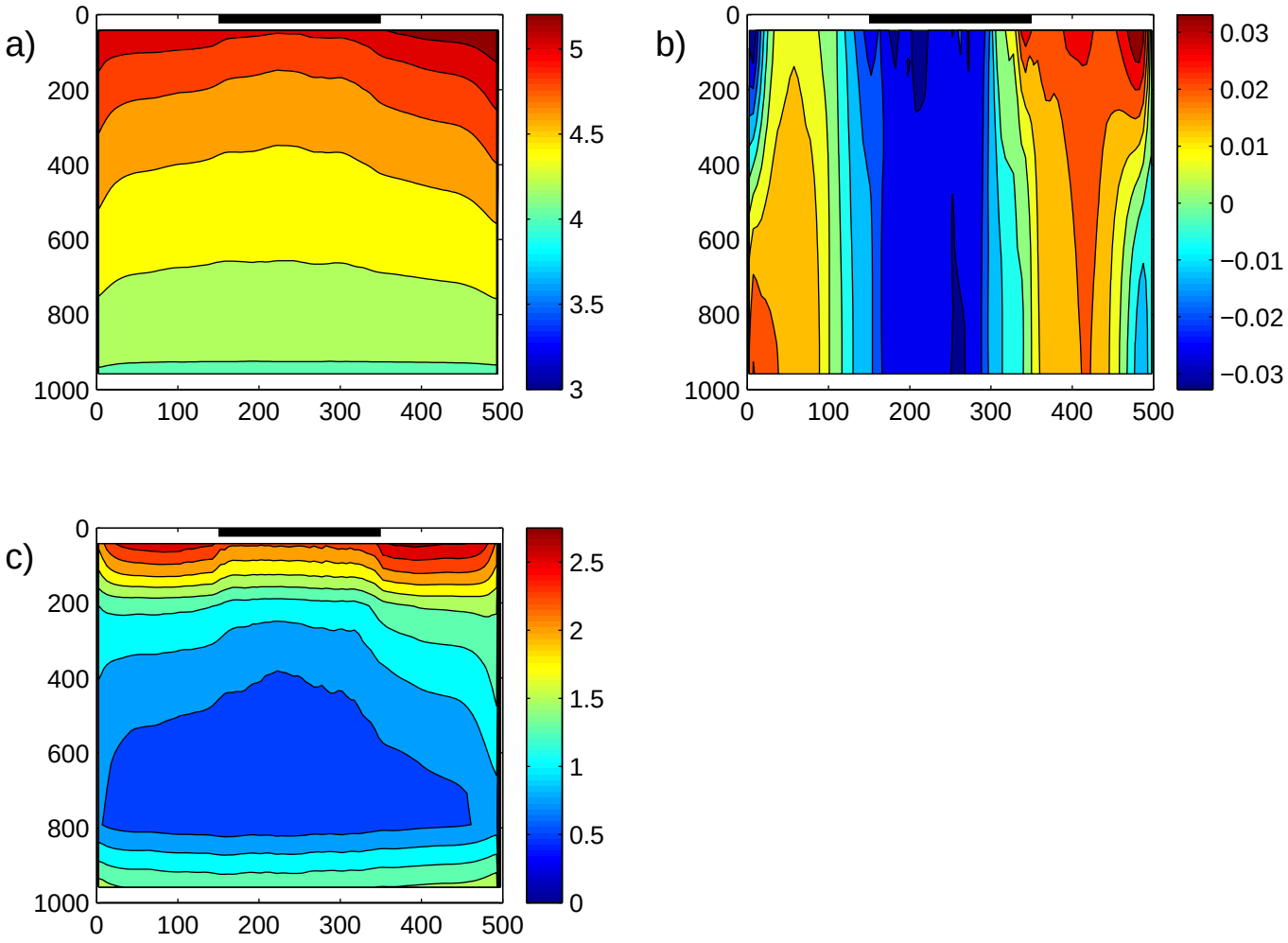

Figure 3: Mean zonal section through the center of the marginal sea a) temperature (° C), b) meridional velocity (m s^{-1}), c) potential vorticity. The bold black line near the surface indicates the region of surface cooling.

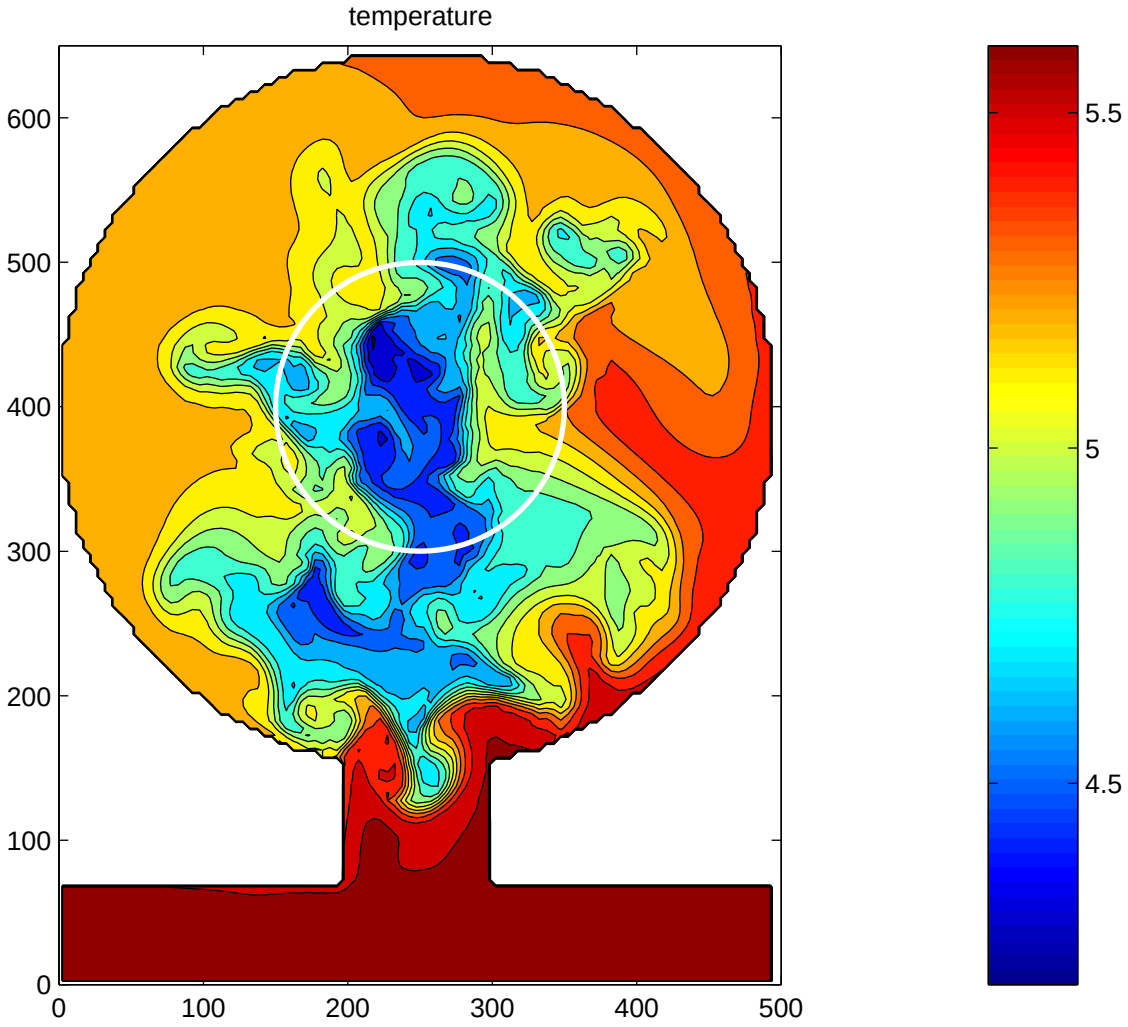

Figure 4: Temperature at 41.7m 10 days after cooling has ceased during year 8.

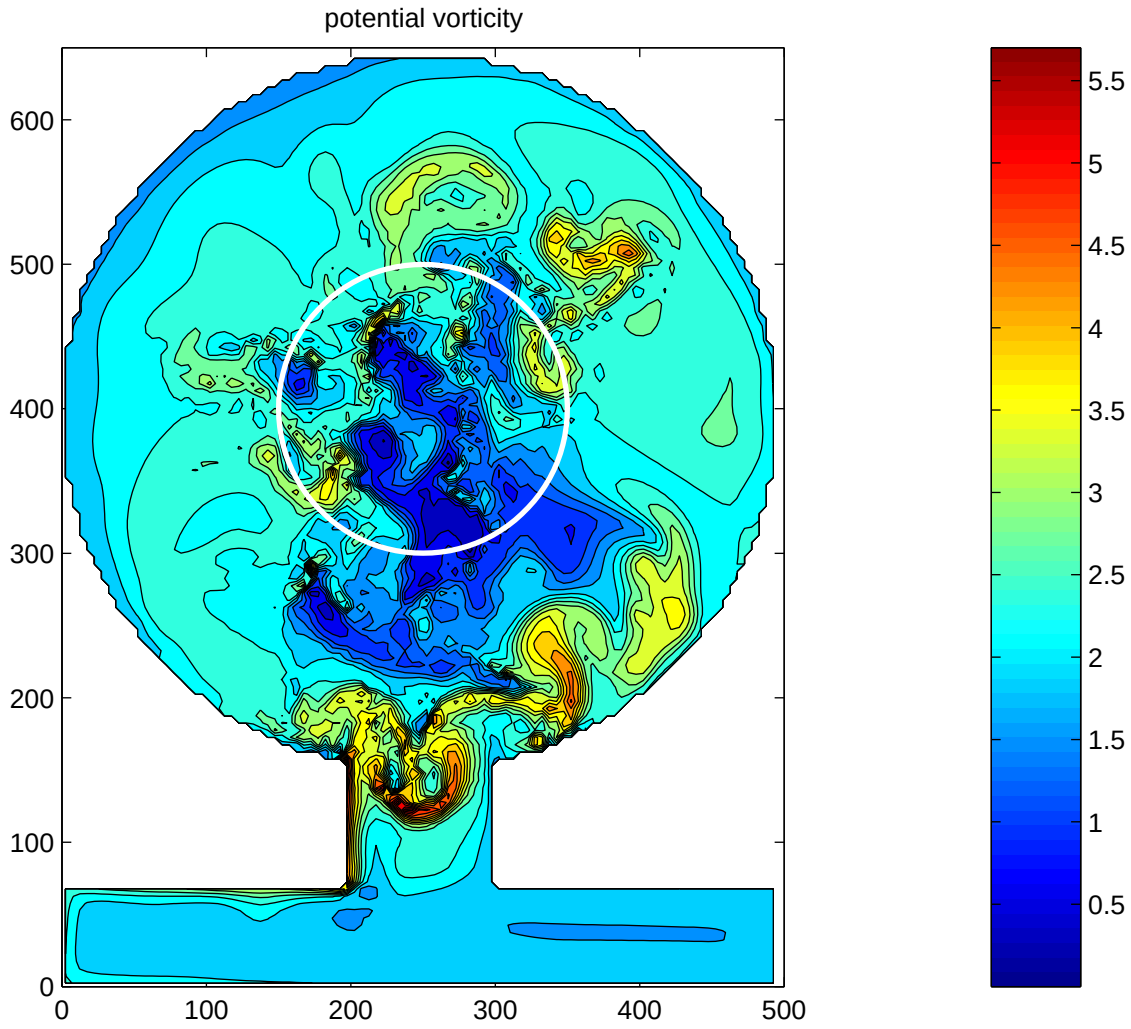

Figure 5: Potential vorticity at 41.7 m 10 days after cooling has ceased during year 8.

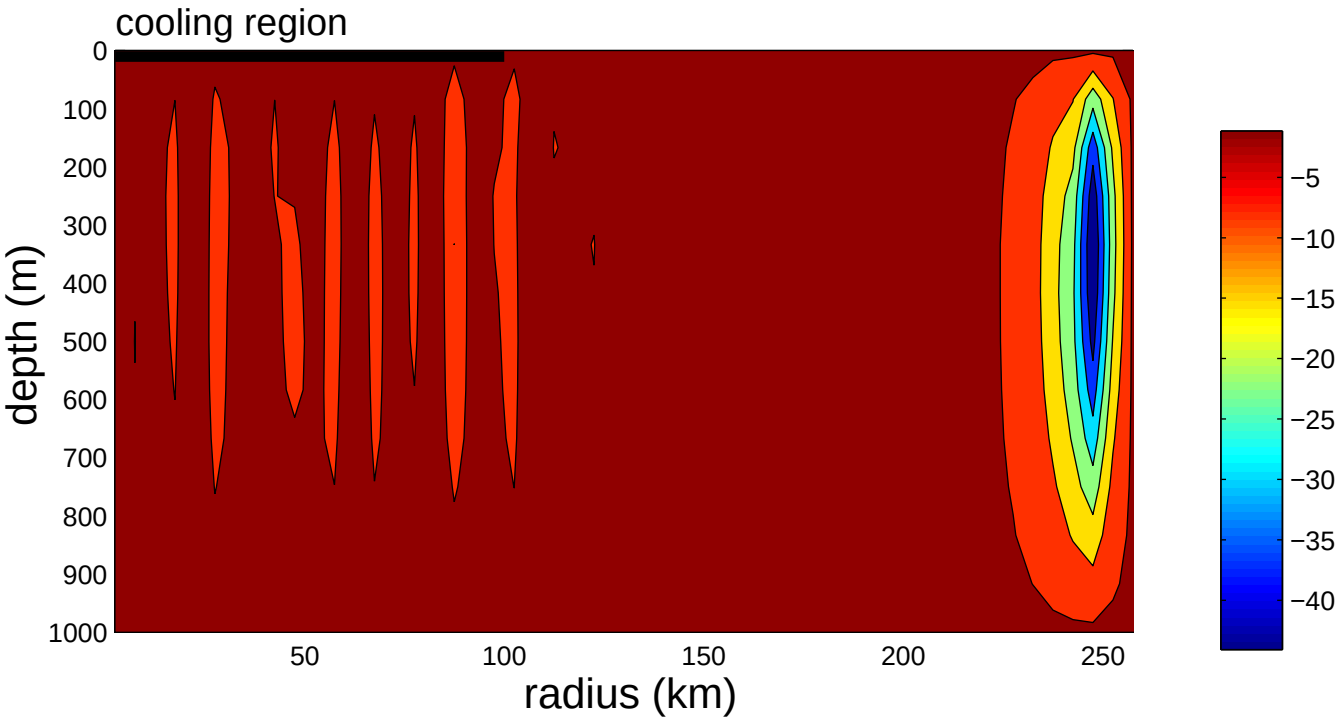

Figure 6: Vertical velocity integrated in the azimuthal direction as a function of depth and radius (m^2 s^{-1}). The bold black line near the surface for radius less than 100 km indicates the region of surface cooling.

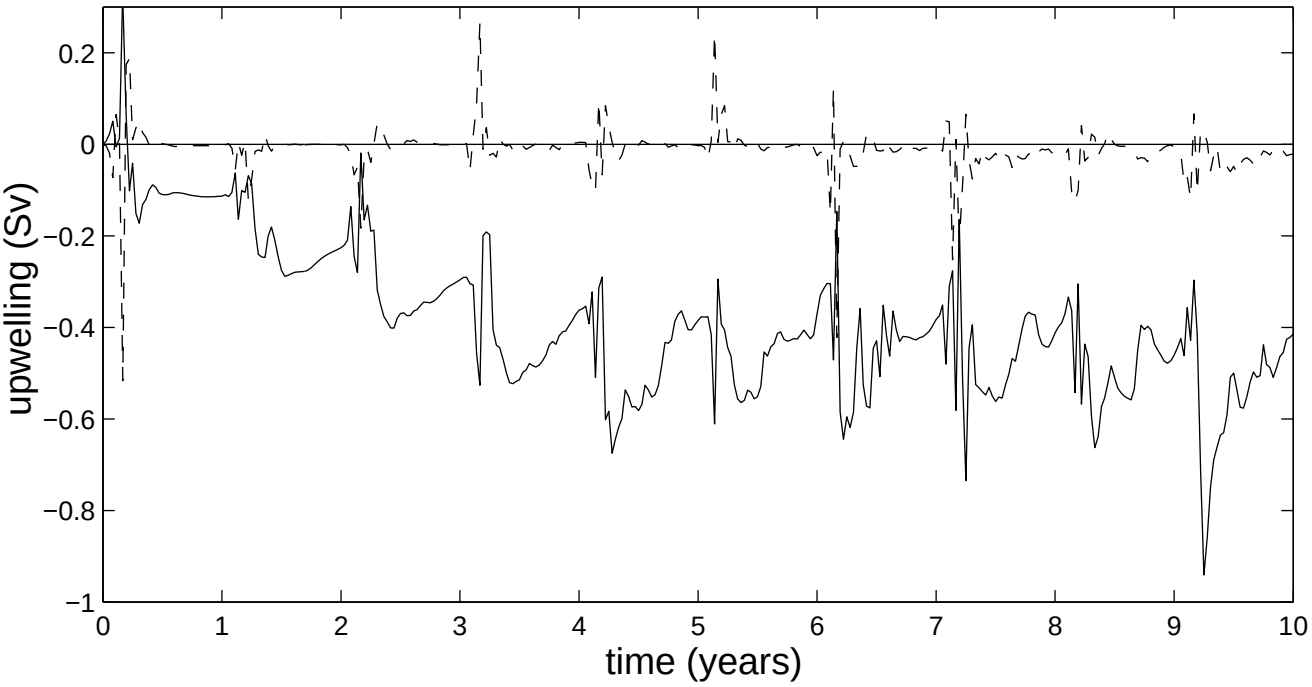

Figure 7: Total upwelling rate within the marginal sea as a function of time (negative downward), 1 Sv = 10^6 m^3 s^{-1}. dashed line : upwelling within the cooling region, radii less than 100 km. solid line : upwelling outside the cooling region, between radii 100 km and 250 km.

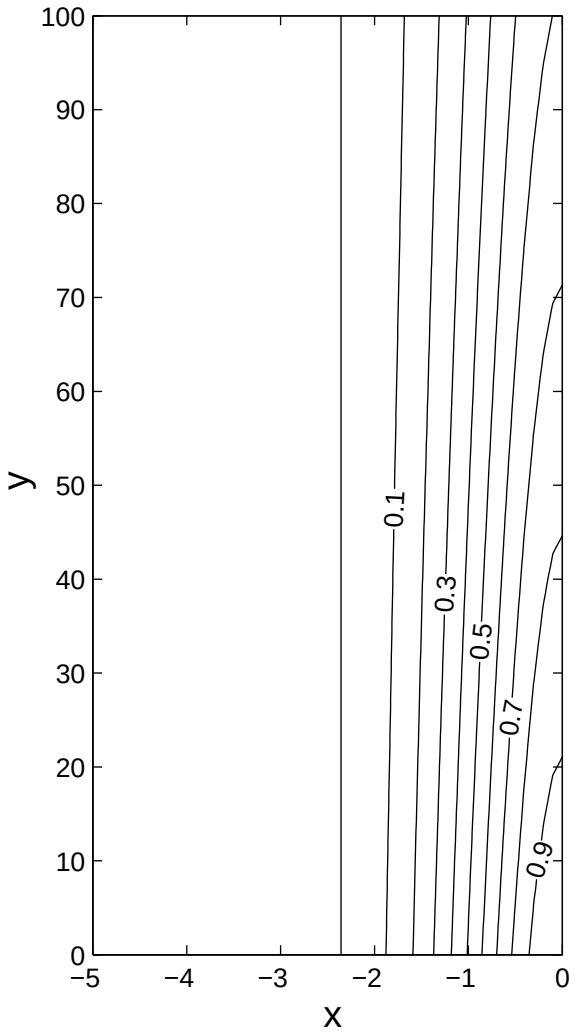

Figure 8: Pressure (or upper layer thickness) from the analytic model.

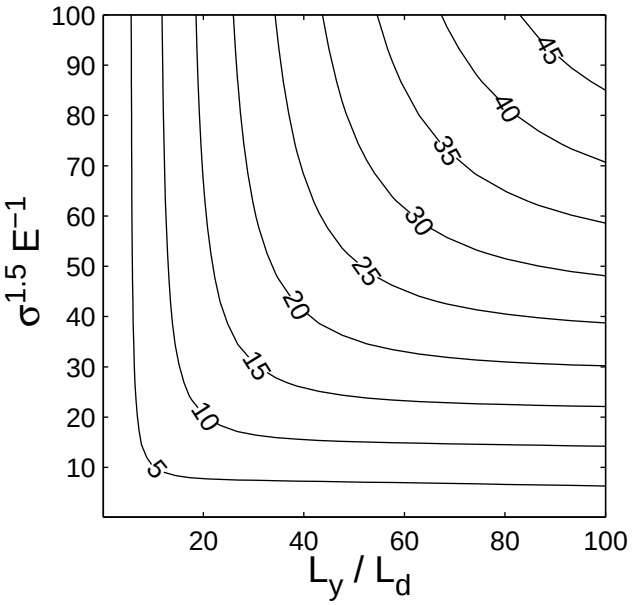

Figure 9: Total nondimensional downwelling rate within a marginal sea as a function of the basin perimeter L_y and the along-boundary decay scale.

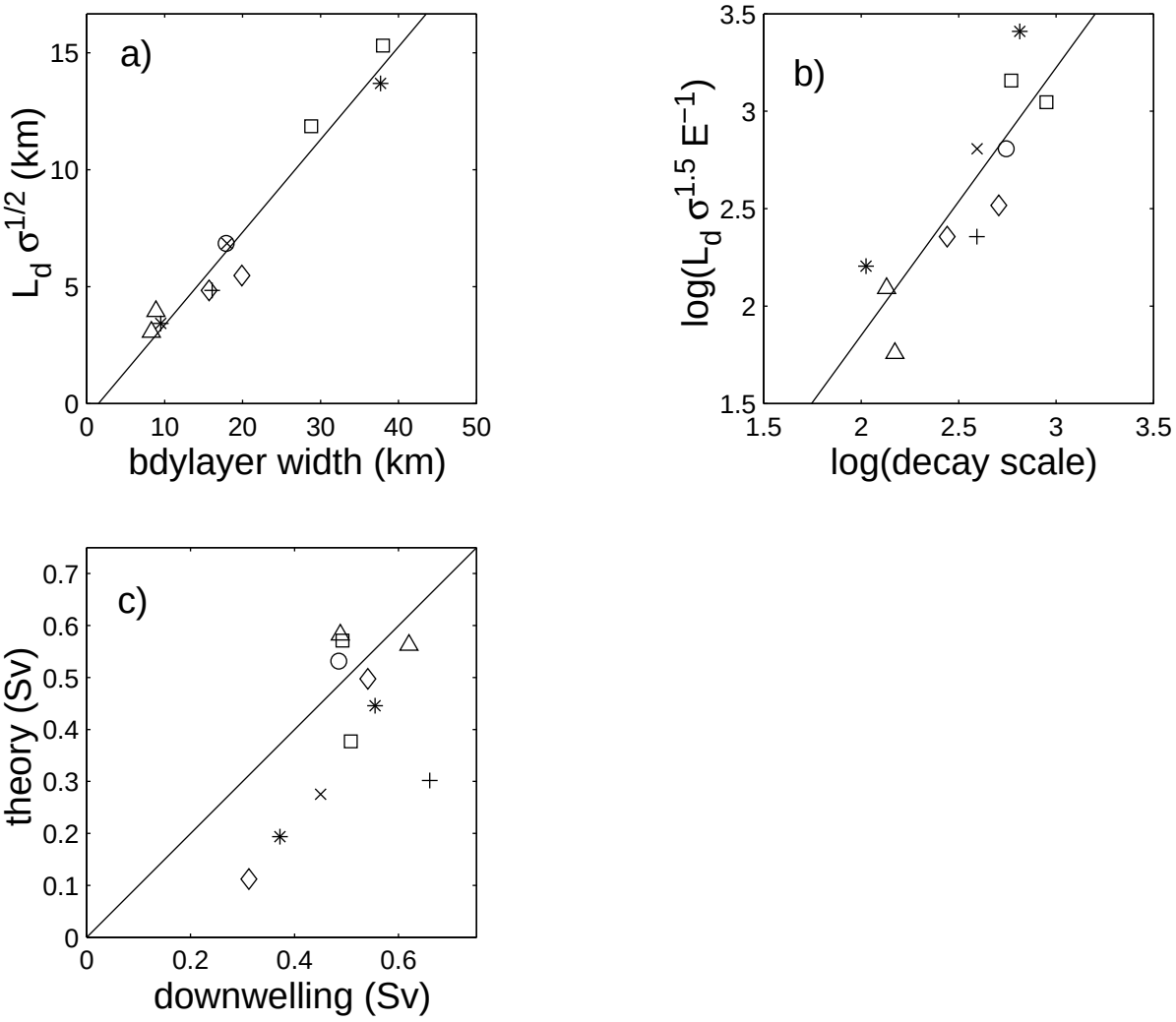

Figure 10: Comparison between a series of numerical model calculations and the theory for a) boundary layer width, b) log of the along-boundary decay scale (km) and c) total downwelling within the basin. The model calculations and corresponding symbols are given in Table 1.

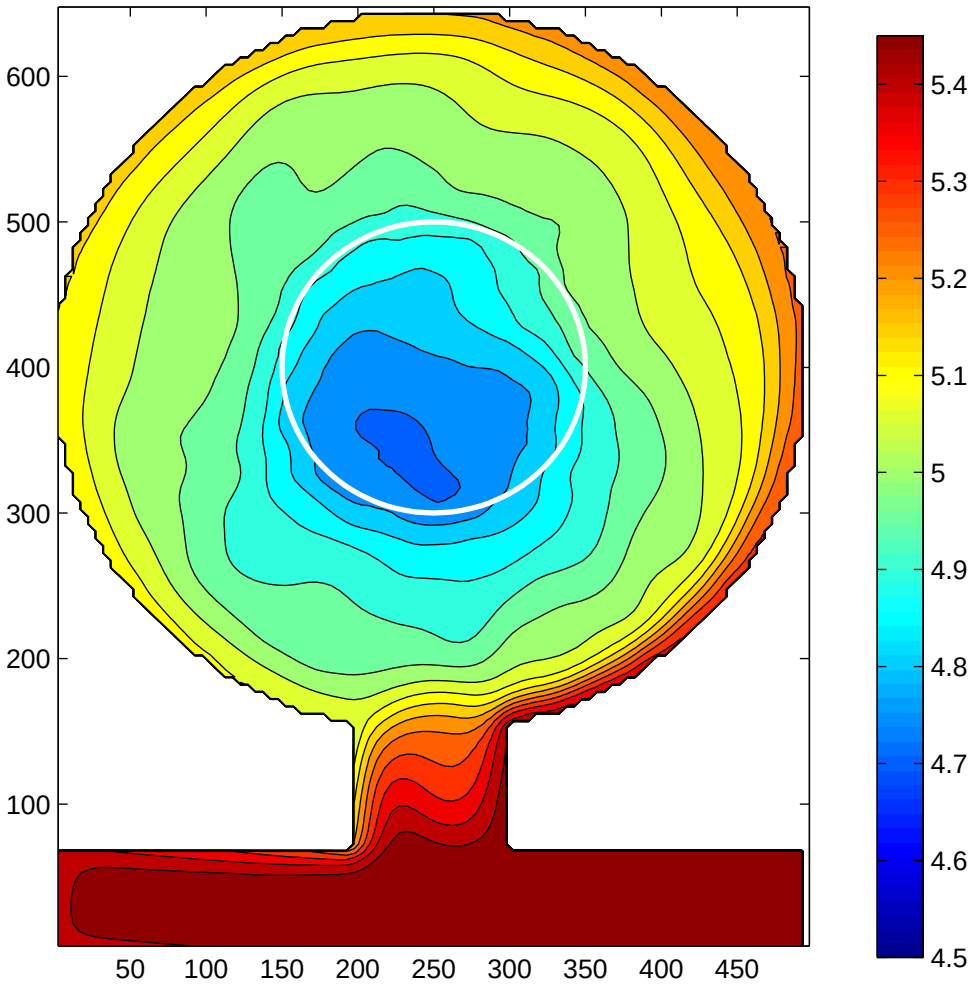

Figure 11: Mean temperature at 41.7 m for $A_h = 150$ m^2 s^{-1} (along-boundary decay scale is 1100 km).

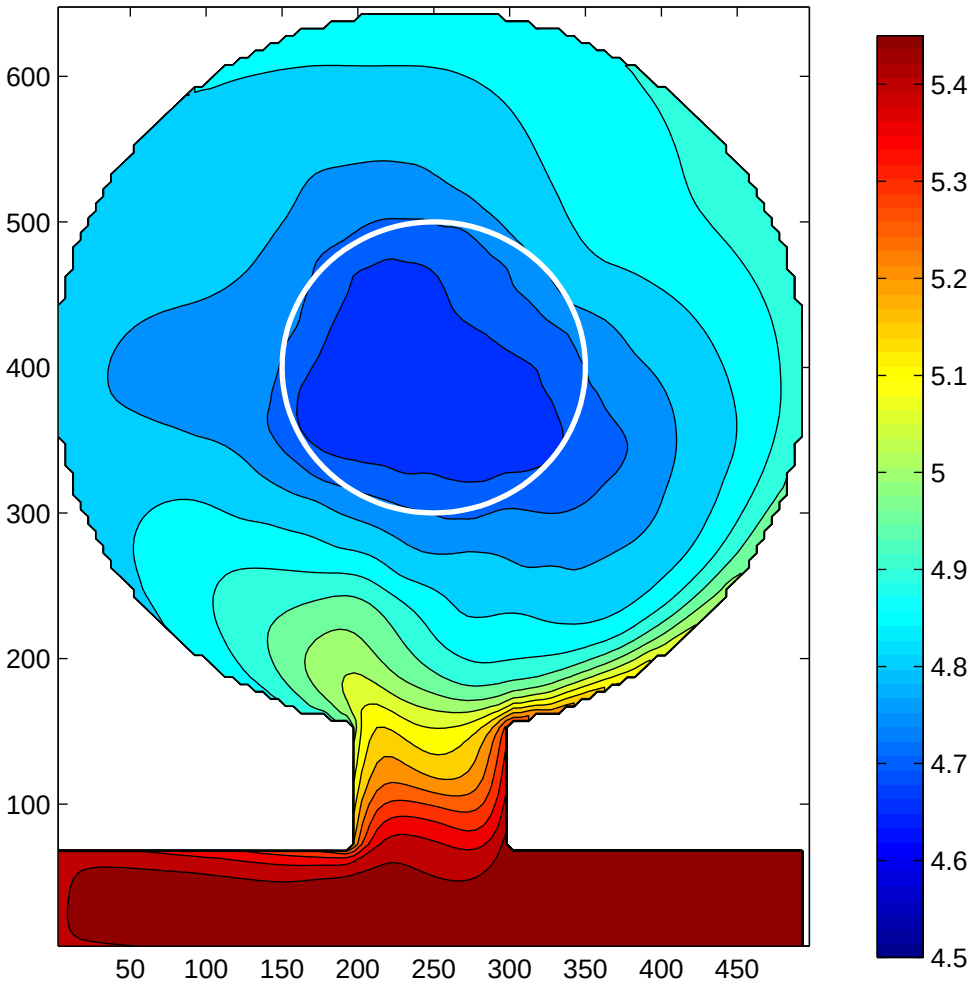

Figure 12: Mean temperature at 41.7 m for $A_T = 150$ m^2 s^{-1} (along-boundary decay scale is 125 km).

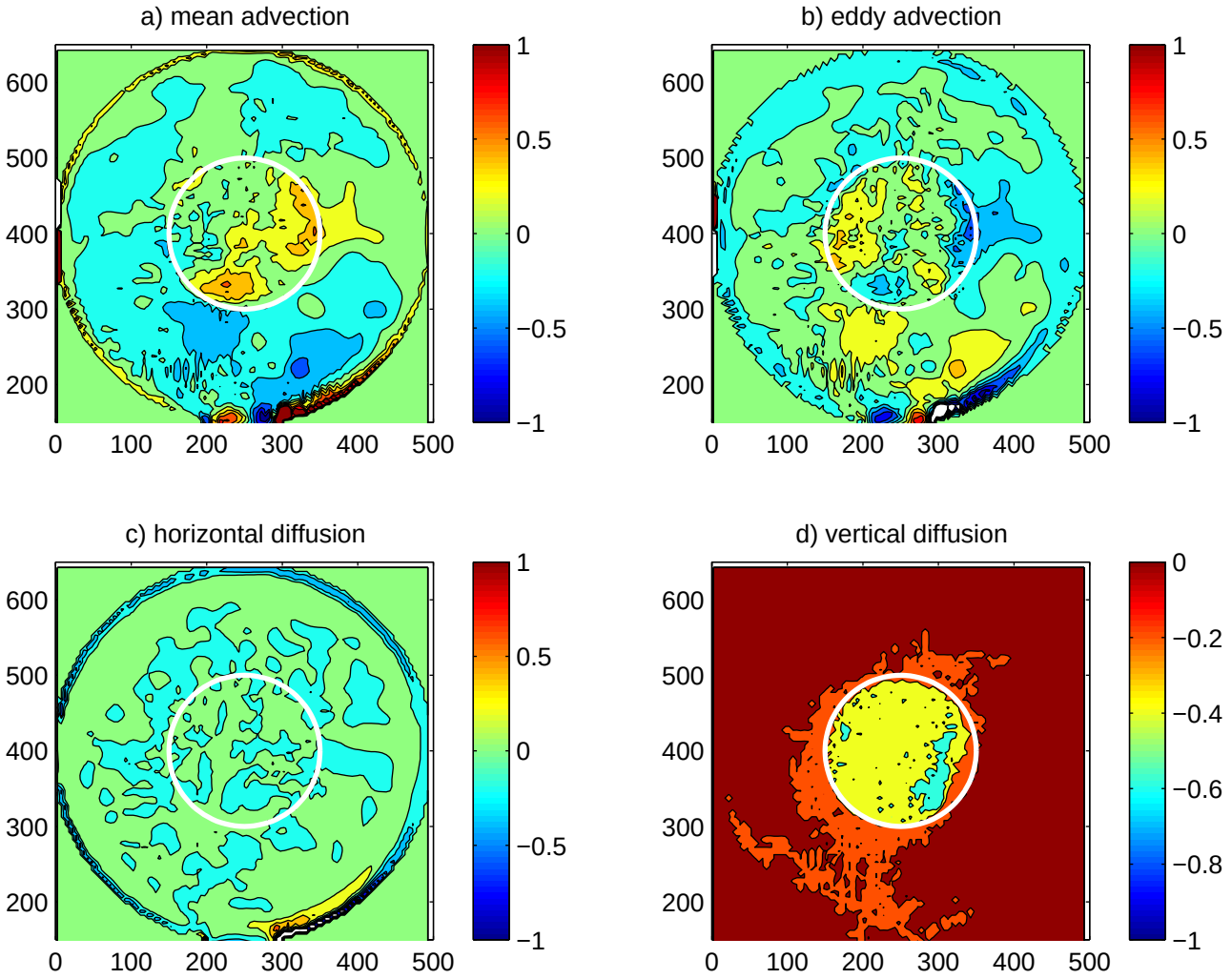

Figure 13: Contributions to the temperature tendency equation at 208 m depth due to a) mean advection, b) eddy advection, c) horizontal diffusion, d) vertical diffusion. The contour interval is 0.2×10^{-7}°C s^{-1}.

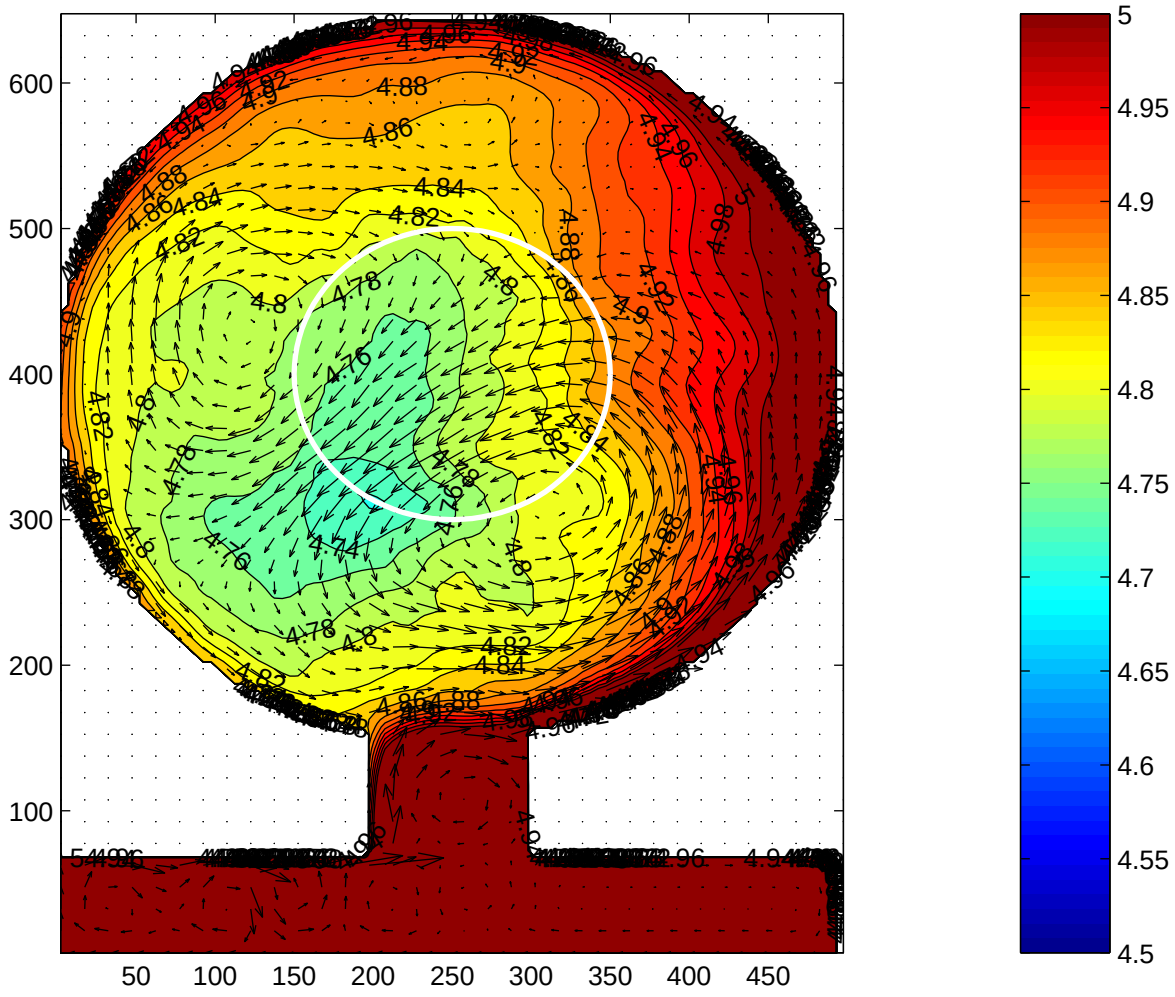

Figure 14: Mean temperature and horizontal velocity calculated between years 7-10 at 208 m depth.

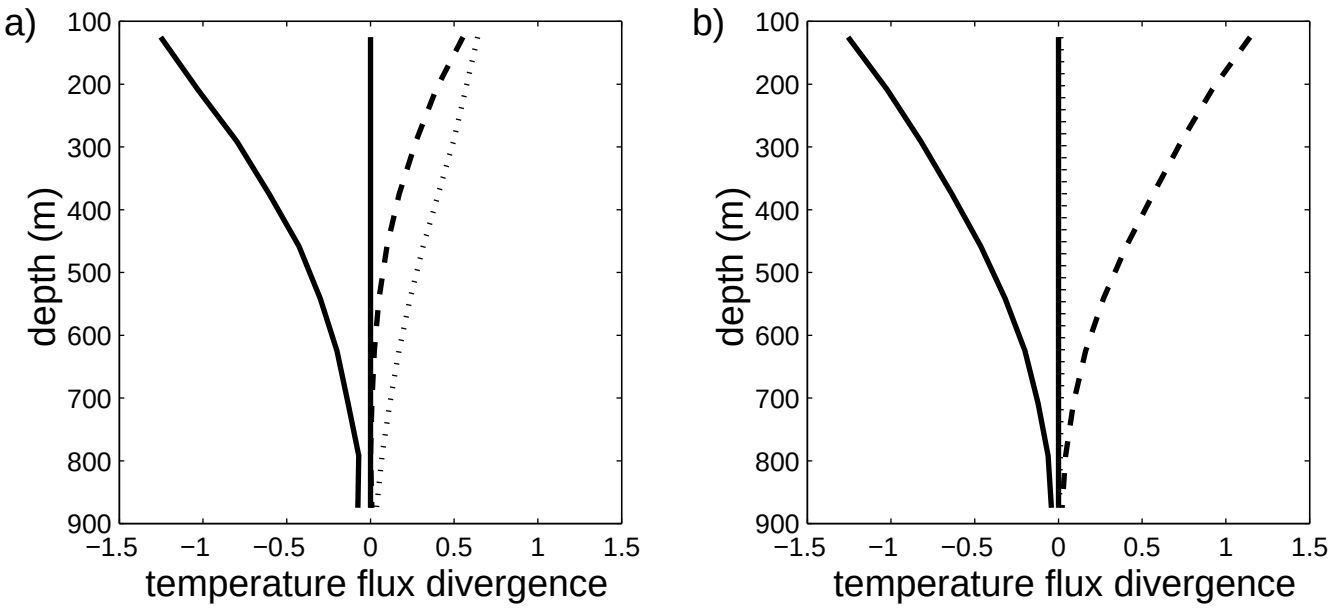

Figure 15: Contributions to the temperature tendency equation integrated over the cooling region as a function of depth. a) calculated between years 7 and 10. b) calculated between years 10 and 30. Units are 10^3 m^2 °C s^{-1}.